crystals

MDPI

Article

Structural and Spectroscopic Effects of Li^+ Substitution for Na^+ in $Li_xNa_{1-x}CaLa_{0.5}Er_{0.05}Yb_{0.45}(MoO_4)_3$ Upconversion Scheelite-Type Phosphors

Chang Sung Lim [1,*], Aleksandr Aleksandrovsky [2,3], Maxim Molokeev [4,5,6], Aleksandr Oreshonkov [7,8,*] and Victor Atuchin [9,10,11,12]

1 Department of Aerospace Advanced Materials and Chemical Engineering, Hanseo University, Seosan 31962, Republic of Korea
2 Laboratory of Coherent Optics, Kirensky Institute of Physics, Federal Research Center KSC SB RAS, 660036 Krasnoyarsk, Russia
3 Institute of Nanotechnology, Spectroscopy and Quantum Chemistry, Siberian Federal University, 660041 Krasnoyarsk, Russia
4 Laboratory of Crystal Physics, Kirensky Institute of Physics, Federal Research Center KSC SB RAS, 660036 Krasnoyarsk, Russia
5 Institute of Engineering Physics and Radioelectronics, Siberian Federal University, 660041 Krasnoyarsk, Russia
6 Department of Physics, Far Eastern State Transport University, 680021 Khabarovsk, Russia
7 Laboratory of Molecular Spectroscopy, Kirensky Institute of Physics, Federal Research Center KSC SB RAS, 660036 Krasnoyarsk, Russia
8 School of Engineering and Construction, Siberian Federal University, 660041 Krasnoyarsk, Russia
9 Laboratory of Optical Materials and Structures, Institute of Semiconductor Physics, SB RAS, 630090 Novosibirsk, Russia
10 Research and Development Department, Kemerovo State University, 650000 Kemerovo, Russia
11 Department of Industrial Machinery Design, Novosibirsk State Technical University, 630073 Novosibirsk, Russia
12 R&D Center "Advanced Electronic Technologies", Tomsk State University, 634034 Tomsk, Russia
* Correspondence: cslim@hanseo.ac.kr (C.S.L.); oreshonkov@iph.krasn.ru (A.O.)

Abstract: New triple molybdates $Li_xNa_{1-x}CaLa_{0.5}(MoO_4)_3$:$Er^{3+}$0.05/$Yb^{3+}$0.45 (x = 0, 0.05, 0.1, 0.2, 0.3) were manufactured successfully using the microwave-assisted sol-gel-based technique (MAS). Their room-temperature crystal structures were determined in space group $I4_1/a$ by Rietveld analysis. The compounds were found to have a scheelite-type structure. In Li-substituted samples, the sites of big cations were occupied by a mixture of (Li, Na, La, Er, Yb) ions, which provided a linear cell volume decrease with the Li content increase. The increased upconversion (UC) efficiency and Raman spectroscopic properties of the phosphors were discussed in detail. The mechanism of optimization of upconversion luminescence upon Li content variation was shown to be due to the control of excitation/energy transfer channel, while the control of luminescence channels played a minor role. The UC luminescence maximized at lithium content x = 0.05. The mechanism of UC optimization was shown to be due to the control of excitation/energy transfer channel, while the control of luminescence channels played a minor role. Over the whole spectral range, the Raman spectra of $Li_xNa_{1-x}CaLa_{0.5}(MoO_4)_3$ doped with Er^{3+} and Yb^{3+} ions were totally superimposed with the luminescence signal of Er^{3+} ions, and increasing the Li^+ content resulted in the difference of Er^{3+} multiple intensity. The density functional theory calculations with the account for the structural disorder in the system of Li, Na, Ca, La, Er and Yb ions revealed the bandgap variation from 3.99 to 4.137 eV due to the changing of Li content. It was found that the direct electronic transition energy was close to the indirect one for all compounds. The determined chromaticity points (ICP) of the $LiNaCaLa(MoO_4)_3$:Er^{3+},Yb^{3+} phosphors were in good relation to the equal-energy point in the standard CIE (Commission Internationale de L'Eclairage) coordinates.

check for updates

Citation: Lim, C.S.; Aleksandrovsky, A.; Molokeev, M.; Oreshonkov, A.; Atuchin, V. Structural and Spectroscopic Effects of Li^+ Substitution for Na^+ in $Li_xNa_{1-x}CaLa_{0.5}Er_{0.05}Yb_{0.45}(MoO_4)_3$ Upconversion Scheelite-Type Phosphors. *Crystals* **2023**, *13*, 362. https://doi.org/10.3390/cryst13020362

Academic Editor: Alessandro Chiasera

Received: 6 February 2023
Revised: 16 February 2023
Accepted: 17 February 2023
Published: 20 February 2023

Keywords: microwave sol-gel synthesis; complex molybdate; scheelite; crystal structure; Raman; frequency up-conversion; band structure

1. Introduction

Complex molybdates are among the most widely studied oxide materials in modern electronics and photonics owing to their excellent performances [1–6]. It was noted that over the past few decades that special research attention was paid to the use of molybdate hosts in the design of new optical and electronic materials [7–12], and the syntheses of efficient rare-earth-containing molybdate-based phosphor materials working in the visible range became a hot topic of solid-state technology because of the possible wide-range cation substitution and related tuning of physical properties [6,8,11–16].

Recently, the compounds with a scheelite-type structure were proposed as efficient phosphor hosts [3,10–12,17–20]. As it can be reasonably assumed, in the disordered scheelite-type structure, the trivalent rare-earth ions could be substituted, at least partially, by different Ln^{3+} ions, and the crystal lattice efficiently could incorporate the ions due to similar radii of Ln^{3+} ions, and that would increase the limit at the appropriate doping level. Among rare-earth ions, the Er^{3+} ion can be used for the infrared to visible light conversion through the frequency up-conversion (UC) process according to its appropriate electronic energy level configuration. The Yb^{3+} ions co-doping can remarkably enhance the UC yield, and it is provided by the efficient $Yb^{3+} \rightarrow Er^{3+}$energy transfer. In this cation pair, the Er^{3+} ion activator is the luminescence center in the UC particles, and the Yb^{3+} sensitizer increases the UC luminescence efficiency [21–25].

The simple and double molybdate crystals are widely applied in photonic and laser technologies because of their specific structural, thermal and electronic characteristics, high chemical stability and excellent spectroscopic properties [3,4,10,26–33]. However, ternary molybdates are less studied, and only several ternary compounds, including scheelite-type ones, have been recently considered [12,18,34–40]. For the practical application of UC photoluminescence in devices and systems, such as three-dimensional displays, lasers, light-emitting elements and biological detectors, the characteristics, such as the homogeneous UC particle size distribution and uniform morphology, need to be reached. Usually, complex molybdates are prepared by a multistep solid-state reaction method, and it requires high temperatures, long heating process and subsequent grinding. The stages may occasionally result in a loss of the emission intensity. In comparison, the sol-gel-based process has some advantages, including high starting atom intermixing, lower calcination temperature, small particle size and a narrow particle size distribution, which are promising for good phosphor characteristics. However, a disadvantage of long gelation time is common for sol-gel process. In comparison to the traditional methods, a very short reaction time, small-sized particles, narrow particle size distribution and high purity of the final polycrystalline product are the characteristics of microwave synthesis. Microwave heating is delivered to the material surface through the convection and/or radiant heating which is transferred to the material bulk via conduction [3,12,14,41–44]. Thus, the microwave sol-gel process is an efficient method that yields high-homogeneity powder products, and it is emerging as a viable alternative approach to the quick synthesis of high-quality crystalline luminescent materials.

In the present study, the $Li_xNa_{1-x}CaLa_{0.5}Er_{0.05}Yb_{0.45}(MoO_4)_3$ compounds with the fixed Er^{3+} and Yb^{3+} contents and x = 0–0.3 were synthesized by the microwave sol-gel method, and the structural and spectroscopic properties were evaluated to determine the effects of Li^+ substitution for Na^+. Previously, the scheelite-type $NaCaLa(MoO_4)_3$:Er,Yb solid solutions were observed and the rare earth element ratio ($La_{0.5}Er_{0.05}Yb_{0.45}$) was determined as optimal to reach strong UC emission [45]. Thus, in the present work, only this rare earth element ratio was selected, and a wide variation of the Li/Na ratio was implemented to elucidate the solid solution range and related spectroscopic effects.

The synthesized products were characterized by scanning electron microscopy (SEM), X-ray diffraction (XRD) analysis and energy-dispersive X-ray spectroscopy (EDS). The spectroscopic properties were comparatively evaluated using Raman spectroscopy and photoluminescence (PL) measurements.

2. Experimental Methods

2.1. Preparation of Chemical Solutions and Phosphor Products

$LiNO_3$, $La(NO_3)_3{\cdot}6H_2O$, $Ca(NO_3)_2{\cdot}4H_2O$, $Na_2MoO_4{\cdot}2H_2O$ of purity 99.0% (Sigma-Aldrich, St. Louis, MO, USA) and $(NH_4)_6Mo_7O_{24}{\cdot}4H_2O$ (Alfa Aesar, Haverhill, MA, USA) of purity 99.0% were employed as the starting reagents. Additionally, for the precise doping levels, $Er(NO_3)_3{\cdot}5H_2O$ and $Yb(NO_3)_3{\cdot}5H_2O$ in purity 99.9% (Sigma-Aldrich, USA) were applied. Normal citric acid (CA) at purity 99.5% was used as received from Daejung Chemicals Company, Republic of Korea. As to other chemical reagents, NH_4OH (A.R.), ethylene glycol (EG, A.R.) and distilled water (DW) were available to approach the transparent chemical solutions.

The nominal compositions of the $Li_xNa_{1-x}CaLa(MoO_4)_3{:}Er^{3+}{}_{0.05}/Yb^{3+}{}_{0.45}$ samples synthesized in the experiment are listed in Table 1. For the Li-free composition, $NaCaLa_{0.5}(MoO_4)_3{:}Er^{3+}{}_{0.05}/Yb^{3+}{}_{0.45}$ ((a) NCLM:EY), 0.4 mol% $Ca(NO_3)_2{\cdot}4H_2O$, 0.2 mol% $Na_2MoO_4{\cdot}2H_2O$ and 0.171 mol% $(NH_4)_6Mo_7O_{24}{\cdot}4H_2O$ were dissolved in one 250 mL. For the second compound, $Li_{0.05}Na_{0.95}CaLa_{0.5}Er_{0.05}Yb_{0.45}(MoO_4)_3$ ((b) LiNCLM:EY-0.05), 0.4 mol% $Ca(NO_3)_2{\cdot}4H_2O$, 0.19 mol% $Na_2MoO_4{\cdot}2H_2O$, 0.02 mol% $LiNO_3$, and 0.171 mol% $(NH_4)_6Mo_7O_{24}{\cdot}4H_2O$ were used. For the third composition, $Li_{0.1}Na_{0.9}CaLa_{0.5}Er_{0.05}Yb_{0.45}(MoO_4)_3$ ((c) LiNCLM:EY-0.1), 0.4 mol% $Ca(NO_3)_2{\cdot}4H_2O$, 0.18 mol% $Na_2MoO_4{\cdot}2H_2O$, 0.04 mol $LiNO_3$ and 0.171 mol% $(NH_4)_6Mo_7O_{24}{\cdot}4H_2O$ were employed. For the fourth compound, $Li_{0.2}Na_{0.8}CaLa_{0.5}Er_{0.05}Yb_{0.45}$-$(MoO_4)_3$ ((d) LiNCLM:EY-0.2), 0.4 mol% $Ca(NO_3)_2{\cdot}4H_2O$, 0.16 mol% $Na_2MoO_4{\cdot}2H_2O$, 0.08 mol% $LiNO_3$ and 0.171 mol% $(NH_4)_6Mo_7O_{24}{\cdot}4H_2O$ were applied. For the fifth compound, $Li_{0.2}Na_{0.8}CaLa_{0.5}Er_{0.05}Yb_{0.45}(MoO_4)_3$ ((e) LiNCLM:EY-0.3), 0.4 mol% $Ca(NO_3)_2{\cdot}4H_2O$, 0.14 mol% $Na_2MoO_4{\cdot}2H_2O$, 0.12 mol% $LiNO_3$ and 0.171 mol% $(NH_4)_6Mo_7O_{24}{\cdot}4H_2O$ were mixed. Each reported reagent mixture was dissolved in a Pyrex glass with the addition of 80 mL 8M NH_4OH and 20 mL EG. In another 250 mL Pyrex glass, the solution of the rare-earth compounds in a fixed stoichiometry of 0.2 mol% $La(NO_3)_3{\cdot}6H_2O$, 0.02 mol% $Er(NO_3)_3{\cdot}5H_2O$ and 0.18 mol% $Yb(NO_3)_3{\cdot}5H_2O$ was prepared by the addition of 100 mL distilled water. Subsequently, the individual two chemical solutions in each sequence for (a)–(e) were co-mixed slowly in a 450 mL Pyrex glass.

Table 1. Abbreviations and chemical compositions for the $Li_xNa_{1-x}CaLa_{0.5}Er_{0.05}Yb_{0.45}(MoO_4)_3$ samples.

Abbreviation	Chemical Composition
NCLM:EY	$NaCaLa_{0.5}Er_{0.05}Yb_{0.45}(MoO_4)_3$
LiNCLM:EY-0.05	$Li_{0.05}Na_{0.95}CaLa_{0.5}Er_{0.05}Yb_{0.45}(MoO_4)_3$
LiNCLM:EY-0.1	$Li_{0.1}Na_{0.9}CaLa_{0.5}Er_{0.05}Yb_{0.45}(MoO_4)_3$
LiNCLM:EY-0.2	$Li_{0.2}Na_{0.8}CaLa_{0.5}Er_{0.05}Yb_{0.45}(MoO_4)_3$
LiNCLM:EY-0.3	$Li_{0.3}Na_{0.7}CaLa_{0.5}Er_{0.05}Yb_{0.45}(MoO_4)_3$

The co-mixed solutions were vigorously stirred and adjusted to pH = 7–8 using CA and 8M NH_4OH. At this time, the molar ratio of CA to the full employed cation metal ions (CM) would be recommended to reach at 2:1. The solutions were slowly heated up to 80–100 °C before microwave treatments. At this stage, the final solutions of about 20–30 mL in volume appeared to be highly transparent sol formations in 450 mL Pyrex glasses. Then, the resultant solutions were moved into a microwave oven (Samsung Company, Republic of Korea, frequency of 2.45 GHz and maximum power of 1250 W). The parameters of the microwave process applied in the present experiment can be found in previous studies [36,38,45]. After the microwave treatment, the black gels dried at 120 °C were ground and annealed at 850 °C

for 16 h in the air atmosphere. The main synthesis steps are shown in Scheme 1. After the annealing stage, the obtained (a) NCLM:EY, (b) LiNCLM:EY-0.05, (c) LiNCLM:EY-0.1, (d) LiNCLM:EY-0.2 and (e) LiNCLM:EY-0.3 powder samples exhibited light pink colors.

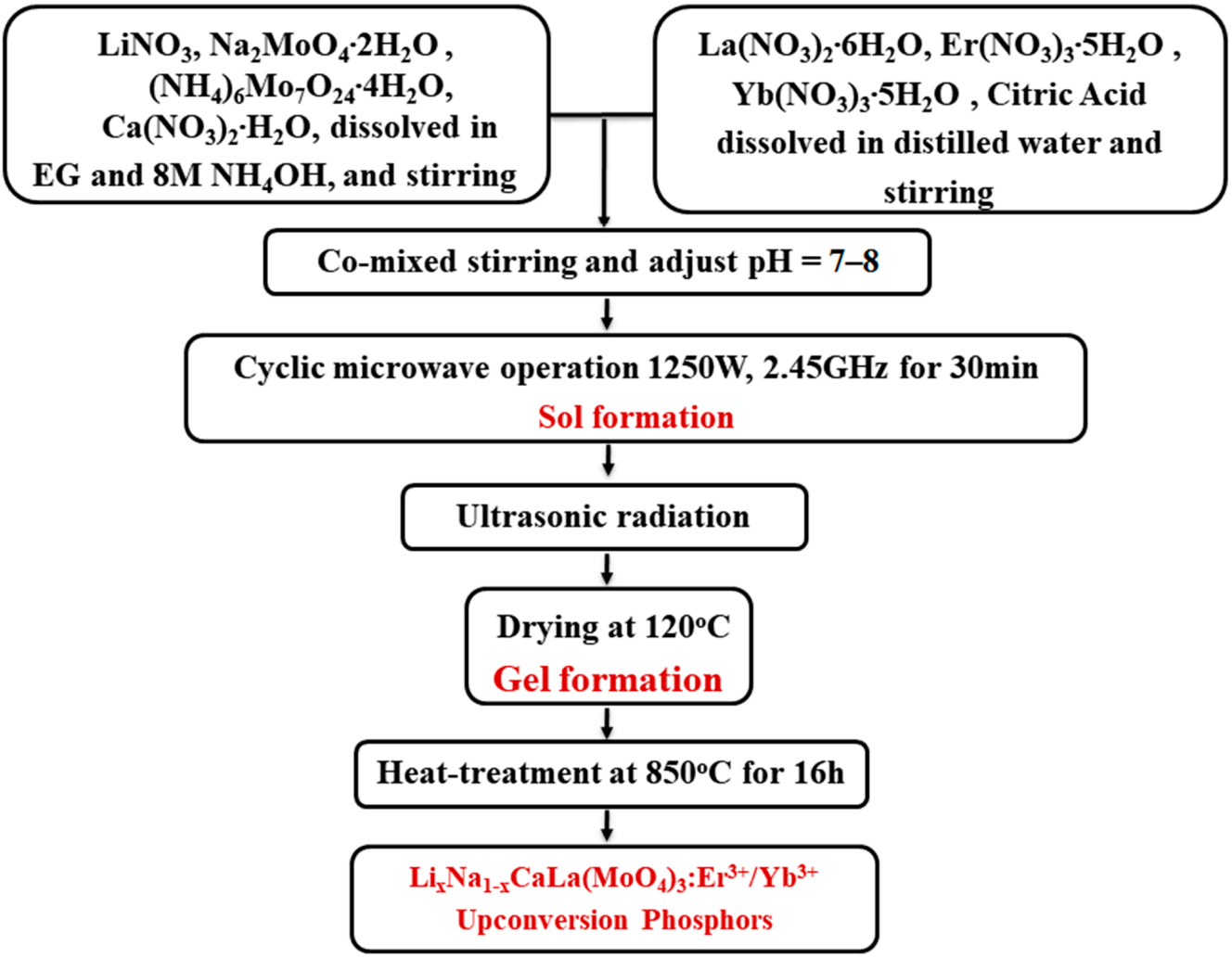

Scheme 1. Flow chart for the synthesis of $LixNa_{1-x}CaLa(MoO_4)_3:Er^{3+}/Yb^{3+}$ UC phosphors by the microwave sol-gel method.

2.2. Characterization

The structural properties of the synthesized powder products $Li_xNa_{1-x}CaLa_{0.5}Er_{0.05}Yb_{0.45}(MoO_4)_3$ were determined using an X-ray (D/MAX 2200, Rigaku, Tokyo, Japan) diffractometer equipped with the Cu Kα radiation (λ = 1.5406 Å) source. The scans were carried out over the diffraction angle range of 2θ = 5–90° at room temperature. The 2θ size step was 0.02°, and the counting time was as long as 5 s per step. For the Rietveld analysis, the TOPAS 4.2 software package was used [46]. The micromorphology of the synthesized particles was observed using scanning electron microscopy (SEM) (JSM-5600, JEOL, Tokyo, Japan). The photoluminescence spectra were acquired at room temperature using a spectrophotometer (Perkin Elmer LS55, Beaconsfield, UK). In the measurements, the samples were excited at 980 nm. The Raman scattering measurements were implemented using a LabRam Aramis (Horiba Jobin-Yvon, Palaiseau, France) device with the spectral resolution of 2 cm^{-1}. The 514.5 nm line of an Ar ion laser was exploited as an excitation source and the power on the sample surface was kept at the 0.5 mW level to avoid the possible sample decomposition.

2.3. Quantum-Chemical Calculations

Quantum-chemical calculations were carried out within the framework of density functional theory (DFT) [47–49] using the CASTEP (Cambridge Serial Total Energy Package) code [50]. The meta-generalized gradient approximation (meta-GGA) and RSCAN [51] (improved version of SCAN [52]) functional were chosen. The on-the-fly generated norm-conserving pseudopotentials [53] with a cutoff energy equal to 800 eV were used for all investigated compounds. The Brillouin zone (BZ) was sampled according to the Monkhorst–Pack scheme [54] with the $4 \times 4 \times 5$ k-point mesh that provided separation of k-points equal to 0.05 $Å^{-1}$. Considering that the structural site of Ca ion was occupied by a mixture of Na, Li, Ca, La, Er and Yb ions with the total occupancy equal to 1, the mixed ion was simulated within the virtual crystal approximation [55]. The tolerance for ground-state wavefunctions founding was chosen to be 2×10^{-6} eV. Pulay density mixing scheme was chosen for electronic minimization.

3. Results and Discussion

3.1. Particle Morphology and Phase Composition

The SEM patterns of the synthesized powder samples are shown in Figures 1 and S1 (see Supplementary Materials). In general, the particle morphologies are similar for all samples. The particles are partly coalescent due to the material diffusion between the grains, and this is typical of oxides subjected to a high temperature annealing [9,56,57]. In all SEM patterns, the biggest grains were ~5–7 μm in size. For comparison, in Figure 1, the SEM patterns are shown for pure NCLM:EY and LiNCLM:EY-0.3 with the highest Li content. In both samples, big grains were mixed with low-sized grains. However, in Figure 1b, the presence of partly faceted big grains is evident and the quantity of low-sized particles was lower. Thus, the presence of Li in the intermediate gels stimulated the grain growth and faceting.

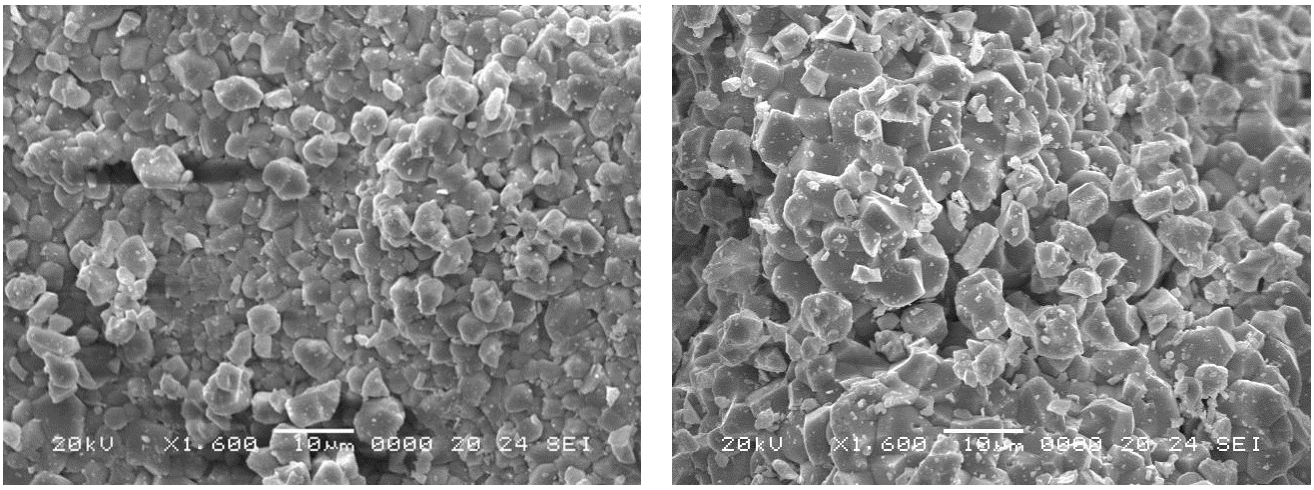

(**a**) (**b**)

Figure 1. SEM patterns recorded for (**a**) NCLM:EY and (**b**) LiNCLM:EY-0.3.

The XRD patterns recorded for the samples are presented in Figures 2 and S2. All peaks were well indexed by the tetragonal cell (space group $I4_1/a$) with the cell parameters close to $CaMoO_4$ (COD 9009632) [58]. There were no alien peaks detected in the patterns, and it meant that all samples were in the pure phase state. Therefore, the $CaMoO_4$ crystal structure was taken as a starting model for the Rietveld refinement. The Ca ion site was considered as that occupied by Na, Li, Ca, La, Er and Yb ions (Figure 3) with fixed occupancies according to nominal compositions. The refinement was stable and gives low *R*-factors (Table 2, Figures 2 and S2). The coordinates of atoms and main bond lengths are

listed in Tables S1 and S2, respectively. The linear increase in cell volume per average ion radii IR (Na/Li/Ca/La/Er/Yb) proves the suggested chemical compositions (Figure 2c).

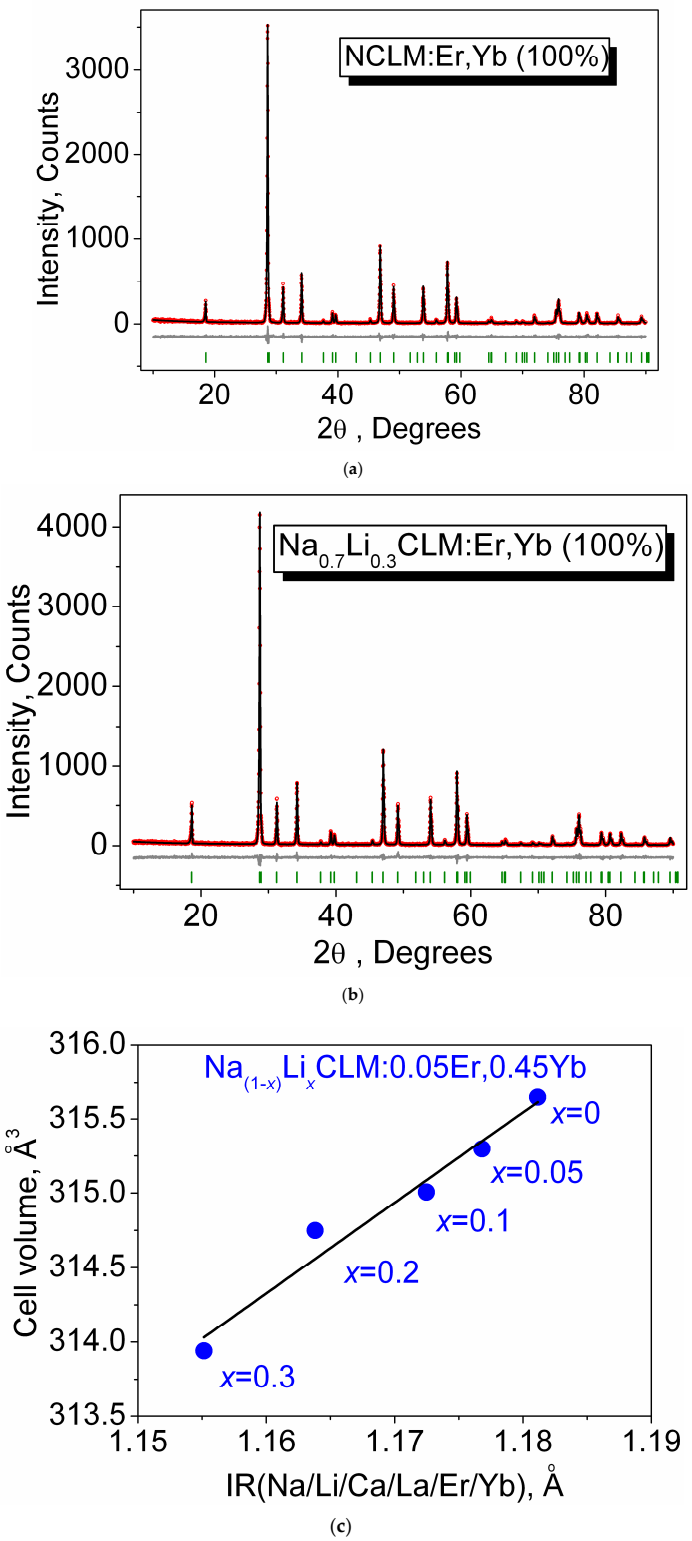

Figure 2. Rietveld difference patterns obtained for (**a**) NCLM:EY and (**b**) LiNCLM:EY-0.3, (**c**) cell volume dependence on x in the $Li_xNa_{1-x}CaLa_{0.5}Er_{0.05}Yb_{0.45}(MoO_4)_3$ solid solutions. Measured points are given in red, calculated profile—in black, difference profile—in grey, and calculated peak positions are shown by segments in green.

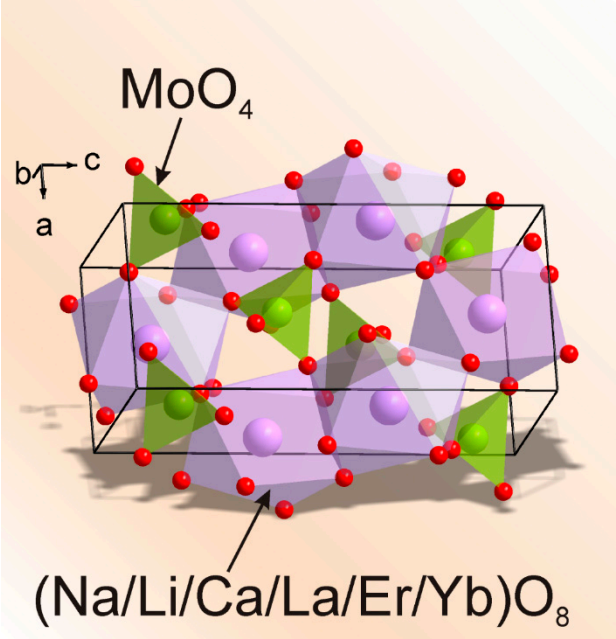

Figure 3. Crystal structure of scheelite-type $Li_xNa_{1-x}CaLa_{0.5}Er_{0.05}Yb_{0.45}(MoO_4)_3$ crystals.

Table 2. Main processing and refinement parameters of the $(Na_{1-x}Li_x)Ca(La_{0.5}Er_{0.05}Yb_{0.45})(MoO_4)_3$ samples.

Compound	Space Group	*Z*	Cell Parameters (Å), Cell Volume (Å^3)	R_p, R_B (%) χ^2
NCLM	$I4_1/a$	4	a = 5.2452 (1) c = 11.4731 (4) V = 315.65 (2)	10.94, 2.04 1.11
$Na_{0.95}Li_{0.05}$CLM: 0.05Er, 0.45Yb	$I4_1/a$	4	a = 5.2432 (1) c = 11.4690 (3) V = 315.30 (2)	9.26, 1.93 1.10
$Na_{0.9}Li_{0.1}$CLM: 0.05Er, 0.45Yb	$I4_1/a$	4	a = 5.2418 (2) c = 11.4646 (4) V = 315.01 (2)	11.10, 2.95 1.12
$Na_{0.8}Li_{0.2}$CLM: 0.05Er, 0.45Yb	$I4_1/a$	4	a = 5.2405 (1) c = 11.4609 (3) V = 314.75 (1)	11.22, 2.82 1.10
$Na_{0.7}Li_{0.3}$CLM: 0.05Er, 0.45Yb	$I4_1/a$	4	a = 5.2364 (1) c = 11.4494 (3) V = 313.94 (2)	10.11, 2.64 1.11

Further details of the crystal structures may be obtained from Fachinformationszentrum Karlsruhe, 76344 Eggenstein-Leopoldshafen, Germany (fax: (+49)7247-808-666; E-mail: crystdata@fiz-karlsruhe.de; http://www.fiz-karlsruhe.de/request_for_deposited_data.html, accessed on 5 February 2023) on quoting the deposition numbers: CSD 2117700-2117704.

The dependence of the unit cell volume on the average ion radius of the cations mixed in the Ca^{2+} site of the $Li_xNa_{1-x}CaLa_{0.5}Er_{0.05}Yb_{0.45}(MoO_4)_3$ solid solutions is shown in Figure 4. For comparison, the cell volume values in $CaMoO_4$ [58], $Na_{0.5}La_{0.5}MoO_4$ [59] and $Na_{1/3}Ca_{1/3}La_{(1-x-y)/3}Er_{x/3}Yb_{y/3}MoO_4$ [45] scheelites are also shown. As can be seen, the previously obtained points of $CaMoO_4$, $Na_{1/3}Ca_{1/3}La_{(1-x-y)/3}Er_{x/3}Yb_{y/3}MoO_4$ and $Na_{0.5}La_{0.5}MoO_4$ were well fitted by the linear function general for the scheelite-type structures. Additionally, the points related to the $Na_{1/3}Ca_{1/3}La_{0.5/3}Er_{0.05/3}Yb_{0.45/3}MoO_4$ composition, as obtained in [45] and in this study, practically coincided, and that verifies high reproducibility of sol-gel microwave synthesis in the application to complex molybdates. However, the points related to Li-containing compositions $Li_{x/3}Na_{(1-x)/3}CaLa_{0.5/3}Er_{0.05/3}Yb_{0.45/3}MoO_4$ form a new branch going strongly away from the straight line general for Li-free scheelites.

For the first time, this structural effect was detected and considered in detail in [39], and it was attributed to a very small radius of the Li^+ ion in reference to the radius of Na^+ ion. Thus, in the present work, this unusual structural effect was observed in one more molybdate system.

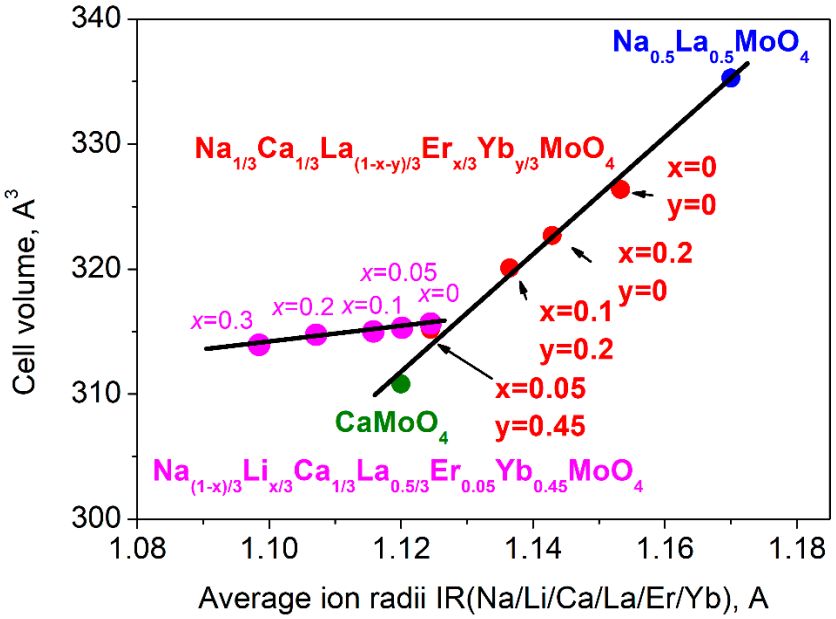

Figure 4. Unit cell volume per averaged ion radii IR(Na/Li/Ca/La/Er/Yb) of $CaMoO_4$ (green) [58], $Na_{1/3}Ca_{1/3}La_{(1-x-y)/3}Er_{x/3}Yb_{y/3}MoO_4$ (red) [45], $Na_{0.5}La_{0.5}MoO_4$ (blue) [59] and $Li_{x/3}Na_{(1-x)/3}CaLa_{0.5/3}Er_{0.05/3}Yb_{0.45/3}MoO_4$ compounds.

3.2. Upconversion Properties

The UC emission spectra of $Na_{1-x}Li_xCaLa(MoO_4)_3$:Er,Yb (x = 0, 0,05, 0.1, 0.2 and 0.3) phosphors excited at 980 nm at room temperature are shown in Figure 5. Under the excitation at 980 nm, Yb^{3+} ions were excited to the $^2F_{5/2}$ state. A pair of excited Yb^{3+} ions transferred their excitation to a single neighboring Er^{3+} ion, thus exciting that Er^{3+} ion to the $^2I_{11/2}$ state. Furthermore, this excitation can be distributed to lower-lying $^4S_{3/2}$ and $^4F_{7/2}$ states. As a result, the upconversion emission of the samples under study exhibited the emission composed of two strong green bands and one weaker red band of the Er^{3+} ion, namely the $^2I_{11/2} \rightarrow {}^4I_{15/2}$, and $^4S_{3/2} \rightarrow {}^4I_{15/2}$ bands in green and $^4F_{7/2} \rightarrow {}^4I_{15/2}$ band in red. The variation of peak intensities of green and red bands, as well as the variation of integral intensity of UC luminescence over the whole spectrum, showed similar behavior on the variation of Li/Na ratio, as seen in Figure 6, all of these dependencies maximizing at comparatively low Li content x = 0.05. The Li^+ ion incorporation into the lattice of hosts instead of larger ions was efficient for manipulating the crystal field affecting the ions positioned within the second coordination sphere of the Li^+ ion or even onto more distant ions. This crystal field manipulation had led to the variation of luminescence of doping ions positioned in the second coordination sphere of the Li^+ ion (see, e.g., [39]. It is highly likely that Li^+ ions did not severely alter the local symmetry of the rare-earth ions in the lattice, but they enabled useful crystal field variations. According to Figure 2c, the cell volume of the solid solution under study monotonically decreases upon the Li^+ content. Thus, in the first approximation, we can expect the monotonical increase in crystal field strengths on Er^{3+} and Yb^{3+} ions. This increase can affect either oscillator strengths in the radiative recombination channels or the efficiency of upconversion excitation process. Hence, there are two ways to optimize the upconversion luminescence, namely (1) to control the full probability of energy transfer from Yb ions to Er ions in the excitation channel or (2) to control the oscillator strengths in the emission channel in order to increase radiative recombination rate against non-radiative one. The similarity of the concentration dependence of upconversion

luminescence (Figure 6) shows that the effect of Li^+ incorporation acts through the efficiency of excitation channel, while changes in the oscillator strengths at luminescence channels lead to a practically unobservable effect.

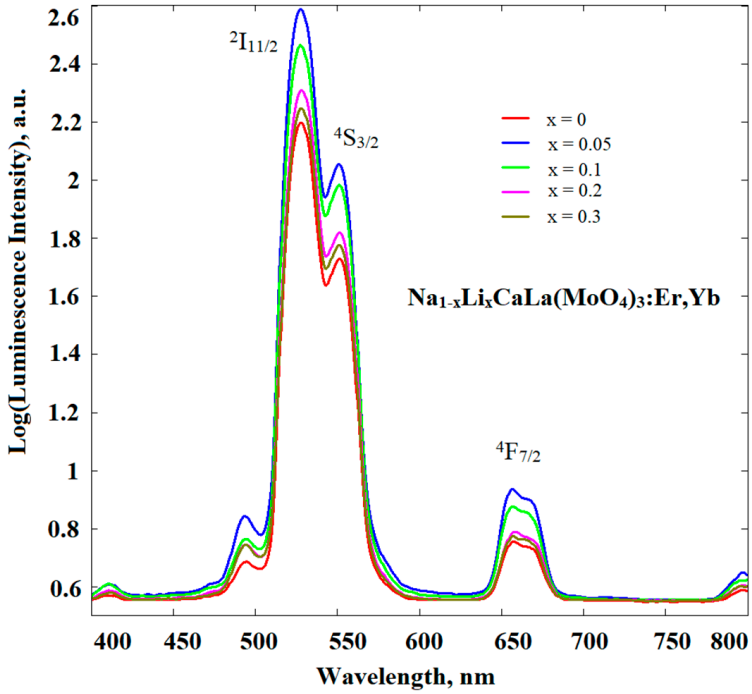

Figure 5. Upconversion luminescence spectra of $Na_{1-x}Li_xCaLa(MoO_4)_3$:Er, Yb. The starting levels for the transitions to the $^4I_{15/2}$ ground state are indicated.

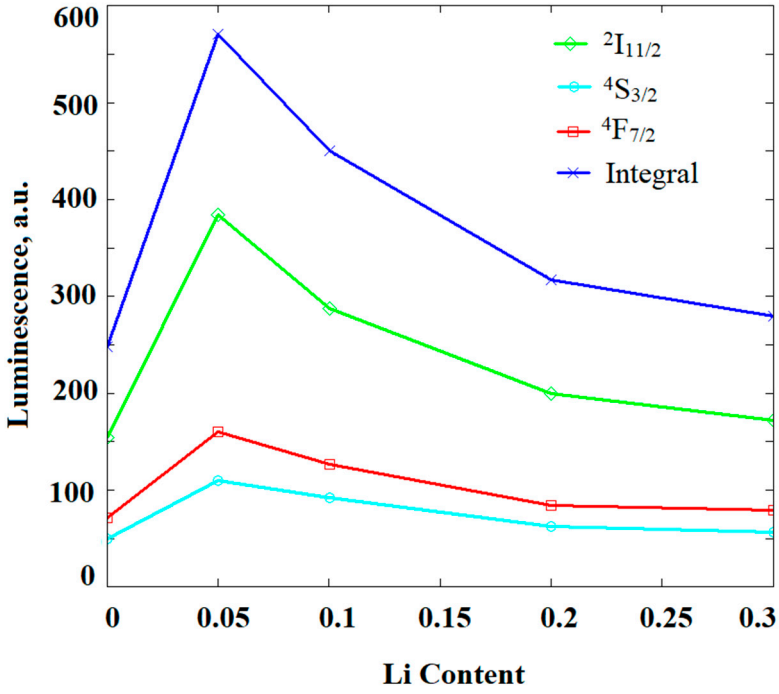

Figure 6. Dependences of intensities of individual UC lines and the integral UC intensity on the Li content in $Na_{1-x}Li_xCaLa(MoO_4)_3$:Er,Yb. The starting levels for the transitions to the $^4I_{15/2}$ ground state are indicated.

3.3. Raman Spectroscopy

The spectral signals recorded from $Na_{1-x}Li_xCaLa(MoO_4)_3$:Er,Yb (x = 0, 0,05, 0.1, 0.2 and 0.3) samples under the excitation of 514.5 nm in the range of Raman-active vibrations are shown in Figure 7. In scheelite-type molybdates, the Raman bands are typically located from 200 to 900 cm^{-1} and they correspond to rotation (around 200 cm^{-1}), bending (from 300 to 450 cm^{-1}) and stretching (700–900 cm^{-1}) vibrations of MoO_4 tetrahedra [3,12,14,18,22,36,38,39,45]. At the same time, the most intense Raman band of scheelite-type molybdates is associated with the symmetrical stretching of $[MoO_4]^{2-}$ ions, and this band is commonly located around 880 cm^{-1}. As can be seen in Figure 7, only a very weak peak was observed in this spectral range in the Raman spectra of $Na_{1-x}Li_xCaLa(MoO_4)_3$:Er,Yb (x = 0, 0,05, 0.1, 0.2 and 0.3) compounds. Such behavior is associated with the fact that the Raman signal is almost totally superimposed by the $^2H_{11/2}$ and $^4S_{3/2}$ luminescence lines of Er^{3+} ions. According to the spectra shown in Figure 7, the variation of peak intensities of $^2H_{11/2}$ bands was different from the UC intensity dependence presented in Figures 5 and 6.

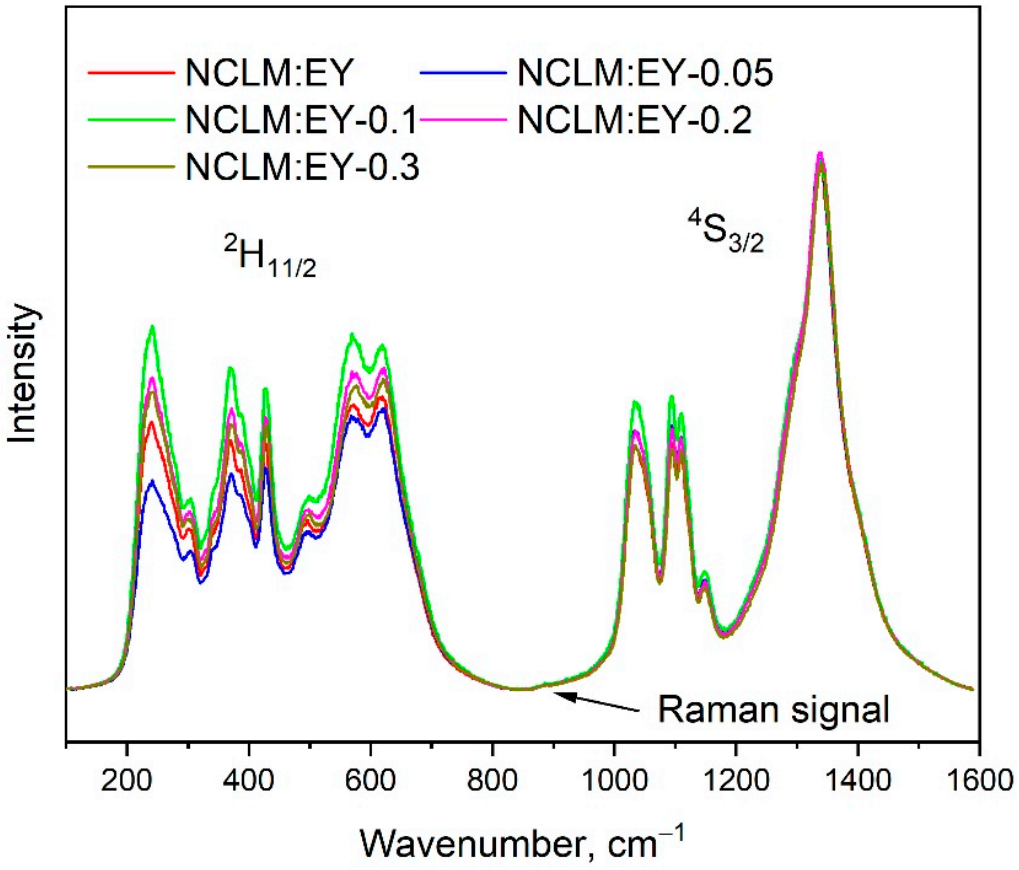

Figure 7. Spectral signal from the $Li_xNa_{1-x}CaLa_{0.5}(MoO_4)_3$: $Er^{3+}{}_{0.05}/Yb^{3+}{}_{0.45}$ samples excited by a 514.5 nm laser line. A very weak Raman peak is marked with the arrow.

3.4. Calculation of Band Structure

The primitive cell of scheelite-type $Li_xNa_{1-x}CaLa_{0.5}Er_{0.05}Yb_{0.45}(MoO_4)_3$ (x = 0–0.3) compounds is shown in Figure 8a and the corresponding Brillouin zone is presented in Figure 8b. The path along the high symmetry points of the BZ should be written as: Γ–X–P–N–Γ–M–S | S_0–Γ | X–R | G–M. The coordinates of these points are: Γ (0, 0, 0), X (0,0,0.5), P (0.25, 0.25, 0.25), N (0, 0.5, 0), M (0.5, 0.5, −0.5), S (0.302, 0.697, −0.302), S_0 (−0.302, 0.302, 0.302), R (−0.104, 0.104, 0.5), G (0.5, 0.5, −0.104).

The dominant part of the DFT simulations of scheelite-type structures is related to $CaMoO_4$ [60–62]. Additionally, the calculation of the band structure for $CaMoO_4$ doped with one ion can be found in several contributions [62,63]. In this work, we implemented

the electronic band structure simulation of $Li_xNa_{1-x}CaLa_{0.5}Er_{0.05}Yb_{0.45}(MoO_4)_3$ (x = 0–0.3) complex compounds using VCA (virtual crystal approximation). The result of the calculation for NCLM:EY is presented in Figure 9a. The band gap value for the direct (optical) electronic transition was 4.0 eV. It should be noted that the obtained values for direct and indirect band gaps differed in the second decimal place only. According to Figure 9b, the valence band top of NCLM:EY was formed by the p-electrons of O, while the conduction band bottom was dominated by the Mo d-electrons. The effects of other cations were minor. Therefore, the transitions that govern the fundamental absorption edge were of charge transfer type and occurred due to the transfer of the O 2p electron to the Mo^{6+} ion within MoO_4 tetrahedra. The energy states of *f* orbitals of Yb and Er ions that are responsible for intraconfigurational f-f transitions and upconversion processes, according to the multiple experimental studies, were all within the bandgap. The band gap values calculated for $Li_xNa_{1-x}CaLa_{0.5}Er_{0.05}Yb_{0.45}(MoO_4)_3$ crystals are presented in Table 3. As is evident, the band gap energy only slightly increased on the Li content increase. An exception was observed for the LiNCLM:EY-0.2 sample. As for this fluctuation, it was revealed that the specific band gap energy value was induced by a slight variation of the O atom coordinates, as determined by the Rietveld refinement.

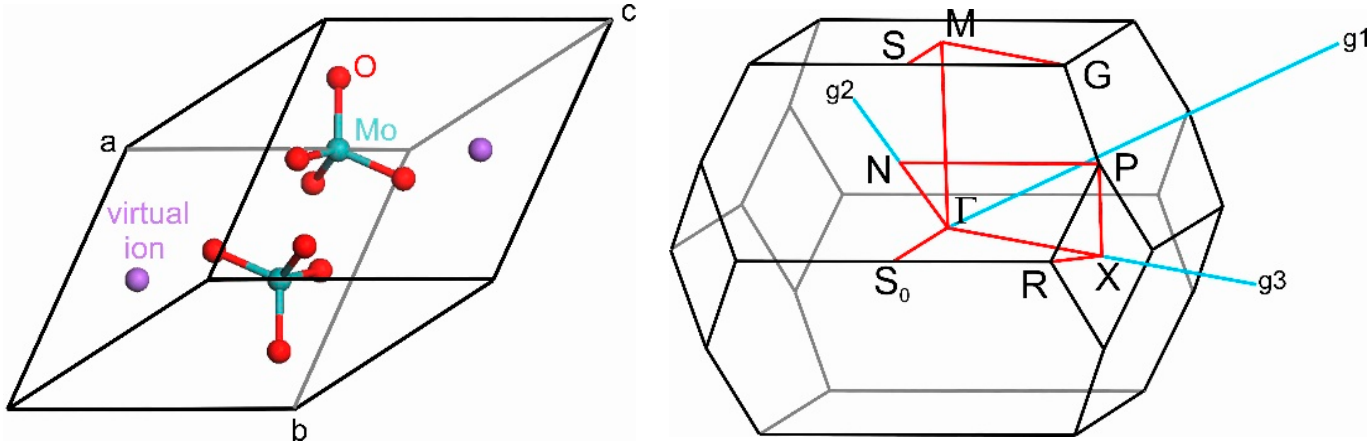

(**a**) (**b**)

Figure 8. Primitive cell (**a**) and Brillouin zone (**b**) of the scheelite-type $Li_xNa_{1-x}CaLa_{0.5}Er_{0.05}Yb_{0.45}$ crystals.

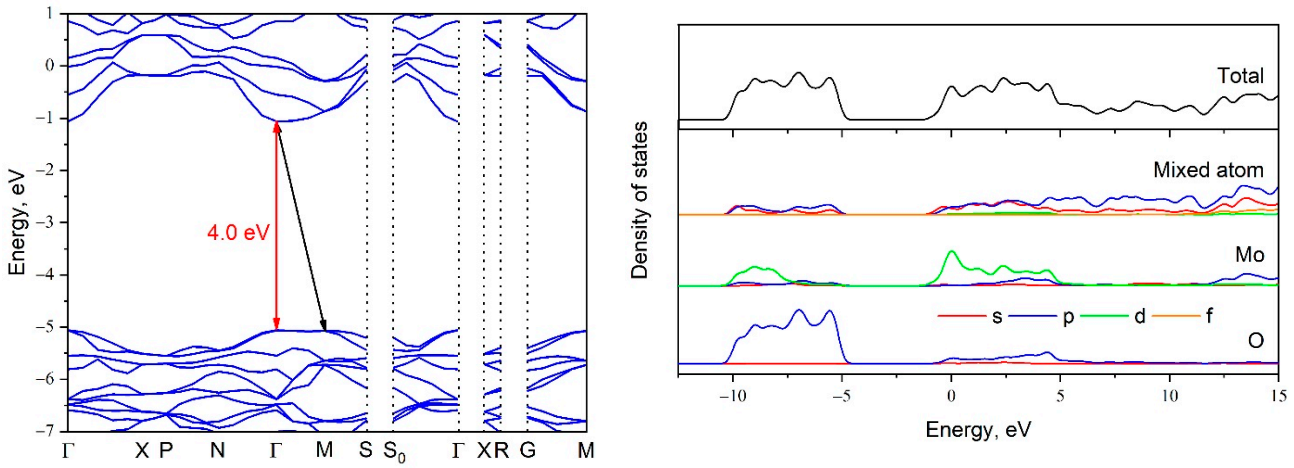

(**a**) (**b**)

Figure 9. Electronic band structure (**a**) and NCLM:EY density of states (**b**).

Table 3. Comparison of calculated band gap values for $Li_xNa_{1-x}CaLa_{0.5}Er_{0.05}Yb_{0.45}(MoO_4)_3$ with data for several scheelite-type structures.

Compound	Source	Calc./Exp.	Band Gap, eV
NCLM:EY	this work	calc.	4.00
LiNCLM:EY-0.05	this work	calc.	4.02
LiNCLM:EY-0.1	this work	calc.	4.12
LiNCLM:EY-0.2	this work	calc.	3.99
LiNCLM:EY-0.3	this work	calc.	4.137
$CaMoO_4$	[62]	calc	2.95
$CaMoO_4$	[60]	calc.	3.2
$CaMoO_4:Eu^{3+}$	[62]	calc	3.35
$CaMoO_4:Tb^{3+}$	[63]	calc	3.96
$CaMoO_4$	[61]	calc.	4.64
$CaMoO_4$	[63]	exp.	3.87
$CaMoO_4$	[60]	exp.	3.9

4. Conclusions

In the present study, the microwave sol-gel method was successfully employed for the preparation of the $Li_xNa_{1-x}CaLa_{0.5}Er_{0.05}Yb_{0.45}(MoO_4)_3$, x = 0–0.3, solid solutions. The compounds were crystallized in tetragonal space group $I4_1/a$, and they are typical representatives of the scheelite crystal family. However, the specific behavior of the structural parameters was observed as a function of the Li content. As the similar effect was previously observed in several related solid solutions with the partial substitution of Li for Na, it can be concluded that an unusual variation of the structural parameters is a general feature of complex Li-containing scheelite-type crystals. Evidently, it could be interesting to search for this effect in other complex scheelites containing big alkaline ions instead of Na.

The upconversion luminescence intensity of $Li_xNa_{1-x}CaLa_{0.5}(MoO_4)_3:Er^{3+}{}_{0.05}/Yb^{3+}{}_{0.45}$ disordered scheelite is optimized via the variation of Li content. It was demonstrated that, in contrast to $Li_xNa_{1-x}CaGd_{0.5}Ho_{0.05}Yb_{0.45}(MoO_4)_3$, which exhibited its non-monotonic variation of the UC intensity upon the Li content, the material under study was featured by a single pronounced maximum of UCL at the Li content x = 0.05. The mechanism that controls the UC intensity was shown to be the variation of probability of energy transfer from Yb ions to Er ions, while the control of the emission channels played an insignificant role. Consequently, these Li-containing phosphors doped with Er^{3+}/Yb^{3+} lead to higher UC emitting efficiency with superior thermal and chemical stabilities overcoming the current limitations of traditional UC materials. It is emphasized that these new UC phosphors can be considered as potentially active optical switching and solar cell devices in practical optoelectronic fields.

Supplementary Materials: The following supporting information can be downloaded at: https://www.mdpi.com/article/10.3390/cryst13020362/s1, Table S1: Fractional atomic coordinates and isotropic displacement parameters ($Å^2$) of the $(Na_{1-x}Li_x)Ca(La_{0.5}Er_{0.05}Yb_{0.45})(MoO_4)_3$ samples; Table S2: Main bond lengths (Å) of the $(Na_{1-x}Li_x)Ca(La_{0.5}Er_{0.05}Yb_{0.45})(MoO_4)_3$ samples; Figure S1: SEM patterns recorded for (a) LiNCLM:EY-0.05, (b) LiNCLM:EY-0.1 and (c) LiNCLM:EY-0.2; Figure S2: Rietveld difference patterns obtained for (a) LiNCLM:EY-0.05, (b) LiNCLM:EY-0.1 and (c) LiNCLM:EY-0.2. Measured points are given in red, calculated profile—in black, difference profile—in grey, and calculated peak positions are shown by segments in green.

Author Contributions: Conceptualization, C.S.L.; methodology, C.S.L.; software, M.M. and A.O.; validation, C.S.L., A.A., M.M., A.O. and V.A.; formal analysis, C.S.L., A.A., M.M., A.O. and V.A.; investigation, C.S.L., A.A., M.M., A.O. and V.A.; resources, C.S.L.; data curation, C.S.L.; writing—original draft preparation, C.S.L., A.A., M.M., A.O. and V.A.; writing—review and editing, C.S.L., A.A., M.M., A.O. and V.A.; visualization, C.S.L., A.A., M.M. and A.O.; supervision, C.S.L.; project administration, C.S.L.; funding acquisition, C.S.L. All authors have read and agreed to the published version of the manuscript.

Funding: This study was funded by the Research Program through the Campus Research Foundation funded by Hanseo University in 2022 (2022046).

Institutional Review Board Statement: Not applicable.

Informed Consent Statement: Not applicable.

Data Availability Statement: Data are available on request.

Conflicts of Interest: The authors declare no conflict of interest.

References

1. Jendoubi, I.; Smail, R.B.; Maczka, M.; Zid, M.F. Optical and electrical properties of the yavapaiite-like molybdate $NaAl(MoO_4)_2$. *Ionics* **2018**, *24*, 3515–3533. [CrossRef]
2. Goulas, A.; Chi-Tangyie, G.; Wang, D.; Zhang, S.; Ketharam, A.; Vaidhyanathan, B.; Reaney, I.M.; Cadman, D.A.; Whittow, W.G.; Vardaxoglou, C.; et al. Microstructure and microwave dielectric properties of 3D printed low loss $Bi_2Mo_2O_9$ ceramics for LTCC applications. *Appl. Mater. Today* **2020**, *21*, 100862. [CrossRef]
3. Lim, C.S.; Aleksandrovsky, A.; Atuchin, V.; Molokeev, M.; Oreshonkov, A. Microwave-employed sol–gel synthesis of scheelite-type microcrystalline $AgGd(MoO_4)_2$:Yb^{3+}/Ho^{3+} upconversion yellow phosphors and their spectroscopic properties. *Crystals* **2020**, *10*, 1000.
4. Sha, X.; Chen, B.; Zhang, X.; Zhang, J.; Xu, S.; Li, X.; Sun, J.; Zhang, Y.; Wang, X.; Zhang, Y.; et al. Pre-assessments of optical transition, gain performance and temperature sensing of Er^{3+} in $NaLn(MoO_4)_2$ (Ln = Y, La, Gd and Lu) single crystals by using their powder-formed samples derived from traditional solid state reaction. *Opt. Laser Technol.* **2021**, *140*, 107012. [CrossRef]
5. Chimitova, O.D.; Bazarov, B.G.; Bazarova, J.G.; Atuchin, V.V.; Azmi, R.; Sarapulova, A.E.; Mikhailova, D.; Balachandran, G.; Fiedler, A.; Geckle, U.; et al. The crystal growth and properties of novel magnetic double molybdate $RbFe_5(MoO_4)_7$ with mixed Fe^{3+}/Fe^{2+} states and 1D negative thermal expansion. *CrystEngComm* **2021**, *23*, 3297–3307. [CrossRef]
6. Wu, F.; Zhou, D.; Du, C.; Xu, D.-M.; Li, R.-T.; Shi, Z.-Q.; Darwish, M.A.; Zhou, T.; Jantunen, H. Design and fabrication of a satellite communication dielectric resonator antenna with novel low loss and temperature-stabilized $(Sm_{1-x}Ca_x)(Nb_{1-x}Mo_x)O_4$ (x = 0.15–0.7) microwave ceramics. *Chem. Mater.* **2023**, *35*, 104–115. [CrossRef]
7. Atuchin, V.V.; Grossman, V.G.; Adichtchev, S.V.; Surovtsev, N.V.; Gavrilova, T.A.; Bazarov, B.G. Structural and vibrational properties of microcrystalline $TlM(MoO_4)_2$ (M = Nd, Pr) molybdates. *Opt. Mater.* **2012**, *34*, 812–816. [CrossRef]
8. Li, T.; Guo, C.; Wua, Y.; Li, L.; Jeong, J.H. Green upconversion luminescence in Yb^{3+}/Er^{3+} co-doped $ALn(MoO_4)_2$ (A = Li, Na and K, Ln = La, Gd and Y). *J. Alloys Compd.* **2012**, *540*, 107–112. [CrossRef]
9. Atuchin, V.V.; Chimitova, O.D.; Adichtchev, S.V.; Bazarov, J.G.; Gavrilova, T.A.; Molokeev, M.S.; Surovtsev, N.V.; Bazarova, Z.G. Synthesis, structural and vibrational properties of microcrystalline β-$RbSm(MoO_4)_2$. *Mater. Lett.* **2013**, *106*, 26–29. [CrossRef]
10. Abakumov, A.M.; Morozov, V.A.; Tsirlin, A.A.; Verbeeck, J.; Hadermann, J. Cation ordering and flexibility of the BO_4^{2-} tetrahedra in incommensurately modulated $CaEu_2(BO_4)_4$ (B = Mo, W) scheelites. *Inorg. Chem.* **2014**, *53*, 9407–9415. [CrossRef]
11. Hao, S.-Z.; Zhou, D.; Hussain, F.; Su, J.-Z.; Liu, W.-F.; Wang, D.-W.; Wang, Q.-P.; Qi, Z.-M. Novel scheelite-type $[Ca_{0.55}(Nd_{1-x}Bi_x)_{0.3}]MoO_4$ ($0.2 \leq x \leq 0.95$) microwave dielectric ceramics with low sintering temperature. *J. Am. Ceram. Soc.* **2020**, *103*, 7259–7266. [CrossRef]
12. Lim, C.S.; Aleksandrovsky, A.S.; Atuchin, V.V.; Molokeev, M.S.; Oreshonkov, A.S. Microwave sol-gel synthesis, microstructural and spectroscopic properties of scheelite-type ternary molybdate upconversion phosphor $NaPbLa(MoO_4)_3$:Er^{3+}/Yb^{3+}. *J. Alloys Compd.* **2020**, *826*, 152095. [CrossRef]
13. Cheng, F.; Xia, Z.; Molokeev, M.S.; Jing, X. Effect of composition modulation on the luminescence properties of Eu^{3+} doped $Li_{1-x}Ag_xLu(MoO_4)_2$ solid-solution phosphors. *Dalton Trans.* **2015**, *44*, 18078–18089. [CrossRef]
14. Lim, C.S.; Aleksandrovsky, A.; Molokeev, M.; Oreshonkov, A.; Atuchin, V. The modulated structure and frequency upconversion properties of $CaLa_2(MoO_4)_4$:Ho^{3+}/Yb^{3+} phosphors prepared by microwave synthesis. *Phys. Chem. Chem. Phys.* **2015**, *17*, 19278–19287. [CrossRef]
15. Xiao, J.; Zhang, W.; Wang, T.; Zhang, J.; Du, H. Photoluminescence enhancement in a $Na_5Y(MoO_4)_4$:Dy^{3+} white-emitting phosphor by partial replacement of MoO_4^{2-} with WO_4^{2-} or VO_4^{3-}. *Ceram. Int.* **2021**, *47*, 12028–12037. [CrossRef]
16. Yu, Y.; Shao, K.; Niu, C.; Liu, L.; Zhu, X.; Wang, Z.; Ma, Z.; Wang, G. Crystal growth, first-principle calculations, optical properties and laser performances toward a molybdate $Er+^3$:$KBaGd(MoO_4)_3$ crystal. *J. Lumin.* **2022**, *252*, 119324. [CrossRef]
17. Lim, C.S.; Atuchin, V.V.; Aleksandrovsky, A.S.; Molokeev, M.S. Preparation of $NaSrLa(WO_4)_3$:Ho^{3+}/Yb^{3+} ternary tungstates and their upconversion photoluminescence properties. *Mater. Lett.* **2016**, *181*, 38–41. [CrossRef]
18. Lim, C.S.; Aleksandrovsky, A.S.; Molokeev, M.S.; Oreshonkov, A.S.; Atuchin, V.V. Microwave synthesis and spectroscopic properties of ternary scheelite-type molybdate phosphors $NaSrLa(MoO_4)_3$:Er^{3+}, Yb^{3+}. *J. Alloys Compd.* **2017**, *713*, 156–163. [CrossRef]
19. Wang, H.; Yamg, T.; Feng, L.; Ning, Z.; Liu, M.; Lai, X.; Gao, D.; Bi, J. Energy transfer and multicolor tunable luminescence properties of $NaGd_{0.5}Tb_{0.5-x}Eu_x(MoO_4)_2$ phosphors for UV-LED. *J. Electron. Mater.* **2018**, *47*, 6494–6506. [CrossRef]

20. Xie, J.; Cheng, L.; Tang, H.; Wang, Z.; Sun, H.; Lu, L.; Mi, X.; Liu, Q.; Zhang, X. Wide range color tunability and efficient energy transfer of novel $NaCaGd(WO_4)_3$:Tb^{3+}, Eu^{3+} phosphors with excellent thermal stability for pc-WLEDs. *Inorg. Chem. Front.* **2021**, *8*, 4517–4527. [CrossRef]
21. Lim, C.S.; Aleksandrovsky, A.; Molokeev, M.; Oreshonkov, A.; Atuchin, V. Microwave sol–gel synthesis and upconversion photoluminescence properties of $CaGd_2(WO_4)_4$:Er^{3+}/Yb^{3+} phosphors with incommensurately modulated structure. *J. Solid State Chem.* **2015**, *228*, 160–166. [CrossRef]
22. Lim, C.S.; Atuchin, V.; Aleksandrovsky, A.; Molokeev, M.; Oreshonkov, A. Microwave sol–gel synthesis of $CaGd_2(MoO_4)_4$:Er^{3+}/Yb^{3+} phosphors and their upconversion photoluminescence properties. *J. Am. Ceram. Soc.* **2015**, *98*, 3223–3230. [CrossRef]
23. Nascimento, J.P.C.; Sales, A.J.M.; Sousa, D.G.; da Silva, M.A.S.; Moreira, S.G.C.; Pavani, K.; Soares, M.J.; Graça, M.P.F.; Kumar, J.S.; Sombra, A.S.B. Temperature-, power-, and concentration-dependent two and three photon upconversion in Er^{3+}/Yb^{3+} co-doped lanthanum ortho-niobate phosphors. *RSC Adv.* **2016**, *6*, 68160–68169. [CrossRef]
24. Krut'ko, V.A.; Komova, M.G.; Pominova, D.V. Synthesis and luminescence of $Gd_{2-x-y}Yb_xEr(Ho)_yGeMoO_8$ germanate-molybdates with scheelite structure. *J. Solid State Chem.* **2020**, *292*, 121704. [CrossRef]
25. Singh, P.; Jain, N.; Shukla, S.; Tiwari, A.K.; Kumar, K.; Singh, J.; Pandey, A.C. Luminescence nanothermometry using a trivalent lanthanide co-doped perovskite. *RSC Adv.* **2023**, *13*, 2939–2948. [CrossRef]
26. Zhang, J.; Gao, Z.; Liu, S.; Zhang, S.; Zhang, W.; Feng, X.; Zhao, P.; He, J.; Tao, X. Simultaneous dual-wavelength operation of β-$BaTeMo_2O_9$ Raman laser at 1320 and 1500 nm. *Appl. Phys. Express* **2013**, *6*, 072702. [CrossRef]
27. Shi, P.; Xia, Z.; Molokeev, M.S.; Atuchin, V.V. Crystal chemistry and luminescence properties of red-emitting $CsGd_{1-x}Eux(MoO_4)_2$ solid-solution phosphors. *Dalton Trans.* **2014**, *43*, 9669–9676. [CrossRef]
28. Zhang, Y.; Cong, H.; Jiang, H.; Li, J.; Wang, J. Flux growth, structure, and physical characterization of new disordered laser crystal $LiNd(MoO_4)_2$. *J. Cryst. Growth* **2015**, *423*, 1–8. [CrossRef]
29. Reshak, A.H.; Alahmed, Z.A.; Bila, J.; Atuchin, V.V.; Bazarov, B.G.; Chimitova, O.D.; Molokeev, M.S.; Prosvirin, I.P.; Yelisseyev, A.P. Exploration of the electronic structure of monoclinic α-$Eu_2(MoO_4)_3$: DFT-based study and X-ray photoelectron spectroscopy. *J. Phys. Chem. C* **2016**, *120*, 10559–10568. [CrossRef]
30. Khyzhun, O.Y.; Bekenev, V.L.; Atuchinb, V.V.; Pokrovsky, L.D.; Shlegel, V.N.; Ivannikova, N.V. The electronic structure of Pb_2MoO_5: First-principles DFT calculations and X-ray spectroscopy measurements. *Mater. Des.* **2016**, *105*, 315–322. [CrossRef]
31. Atuchin, V.V.; Aleksandrovsky, A.S.; Molokeev, M.S.; Krylov, A.S.; Oreshonkov, A.S.; Zhou, D. Structural and spectroscopic properties of self-activated monoclinic molybdate $BaSm_2(MoO_4)_4$. *J. Alloys Compd.* **2017**, *729*, 843–849. [CrossRef]
32. Solodovnikov, S.F.; Atuchin, V.V.; Solodovnikova, Z.A.; Khyzhun, O.Y.; Danylenko, M.I.; Pishchur, D.P.; Plyusnin, P.E.; Pugachev, A.M.; Gavrilova, T.A.; Yelisseyev, A.P.; et al. Synthesis, structural, thermal, and electronic properties of palmierite-related double molybdate α-$Cs_2Pb(MoO_4)_2$. *Inorg. Chem.* **2017**, *56*, 3276–3286. [CrossRef]
33. Ren, H.; Li, H.; Zou, Y.; Deng, H.; Peng, Z.; Ma, T.; Ding, S. Growth and properties of Pr^{3+}-doped $NaGd(MoO_4)_2$ single crystal: A promising InGaN laser-diode pumped orange-red laser crystal. *J. Lumin.* **2022**, *249*, 119034. [CrossRef]
34. Savina, A.A.; Atuchin, V.V.; Solodovnikov, S.F.; Solodovnikova, Z.A.; Krylov, A.S.; Maximovskiy, E.A.; Molokeev, M.S.; Oreshonkov, A.S.; Pugachev, A.M.; Khaikina, E.G. Synthesis, structural and spectroscopic properties of acentric triple molybdate $Cs_2NaBi(MoO_4)_3$. *J. Solid State Chem.* **2015**, *225*, 53–58. [CrossRef]
35. Mhiri, M.; Badri, A.; Amara, M.B. Synthesis and crystal structure of $NaMgFe(MoO_4)_3$. *Acta Crystallogr. Sect. E Crystallogr. Commun.* **2016**, *E72*, 864–867. [CrossRef]
36. Lim, C.S. Synthesis of $NaCaLa(MoO_4)_3$:Ho^{3+}/Yb^{3+} phosphors via microwave sol-gel route and their upconversion photoluminescence properties. *Korean J. Mater. Res.* **2016**, *26*, 363–369. [CrossRef]
37. Rajendran, M.; Vaidyanathan, S. New red emitting phosphors $NaSrLa(MO_4)_3$:Eu^{3+} [M = Mo and W] for white LEDs: Synthesis, structural and optical study. *J. Alloys Compd.* **2019**, *789*, 919–931. [CrossRef]
38. Lim, C.S. Synthesis of microcrystalline $LiNaCaLa(MoO_4)_3$:Yb^{3+}/Ho^{3+} upconversion phosphors and effect of Li^+ on their spectroscopic properties. *Trans. Electr. Electron. Mater.* **2019**, *20*, 60–66. [CrossRef]
39. Lim, C.-S.; Aleksandrovsky, A.; Molokeev, M.; Oreshonkov, A.; Atuchin, V. Structural and spectroscopic effects of Li^+ substitution for Na^+ in $Li_xNa_{1-x}CaGd_{0.5}Ho_{0.05}Yb_{0.45}(MoO_4)_3$ scheelite-type upconversion phosphors. *Molecules* **2021**, *26*, 7357. [CrossRef]
40. Yu, Y.; Shao, K.; Zhu, X.; Zhang, X.; Qiu, H.; Wu, S.; Wang, G. Research on a novel molybdate Er^{3+}:$KBaY(MoO_4)_3$ crystal as a prominent 1.55 μm laser medium. *J. Lumin.* **2021**, *237*, 118194. [CrossRef]
41. Ryu, J.H.; Yoon, J.-W.; Lim, C.S.; Shim, K.B. Microwave-assisted synthesis of barium molybdate by a citrate complex method and oriented aggregation. *Mater. Res. Bull.* **2005**, *40*, 1468–1476. [CrossRef]
42. Rybakov, K.I.; Olevsky, E.A.; Krikun, E.V. Microwave sintering: Fundamentals and modeling. *J. Am. Ceram. Soc.* **2013**, *96*, 1003–1020. [CrossRef]
43. Kitchen, H.J.; Vallance, S.R.; Kennedy, J.L.; Tapia-Ruiz, N.; Carassiti, L.; Harrison, A.; Whittaker, A.G.; Drysdale, T.D.; Kingman, S.W.; Gregory, D.H. Modern microwave methods in solid-state inorganic materials chemistry: From fundamentals to manufacturing. *Chem. Rev.* **2014**, *114*, 1170–1206. [CrossRef]
44. Perera, S.S.; Munasinghe, H.N.; Yatooma, E.N.; Rabuffetti, F.A. Microwave-assisted solid-state synthesis of $NaRE(MO_4)_2$ phosphors (RE = La, Pr, Eu, Dy; M = Mo, W). *Dalton Trans.* **2020**, *49*, 7914–7919. [CrossRef]

45. Lim, C.S.; Aleksandrovsky, A.S.; Molokeev, M.S.; Oreshonkov, A.S.; Ikonnikovg, D.A.; Atuchin, V.V. Triple molybdate scheelite-type upconversion phosphor $NaCaLa(MoO_4)_3:Er^{3+}/Yb^{3+}$: Structural and spectroscopic properties. *Dalton Trans.* **2016**, *45*, 15541–15551. [CrossRef]
46. Bruker. *Bruker AXS TOPAS V4: General Profile and Structure Analysis Software for Powder Diffraction Data—User's Manual*; Bruker AXS: Karlsruhe, Germany, 2008.
47. Hohenberg, P.; Kohn, W. Inhomogeneous electron gas. *Phys. Rev.* **1964**, *136*, B864–B871. [CrossRef]
48. Kohn, W.; Sham, L. Self-consistent equations including exchange and correlation effects. *Phys. Rev.* **1965**, *140*, A1133–A1138. [CrossRef]
49. Oreshonkov, A.S. SI: Advances in density functional theory (DFT) studies of solids. *Materials* **2022**, *15*, 2099. [CrossRef]
50. Clark, S.J.; Segall, M.D.; Pickard, C.J.; Hasnip, P.J.; Probert, M.I.J.; Refson, K.; Payne, M.C. First principles methods using CASTEP. *Z. Für Krist. Cryst. Mater.* **2005**, *220*, 567–570. [CrossRef]
51. Bartók, A.P.; Yates, J.R. Regularized SCAN functional. *J. Chem. Phys.* **2019**, *150*, 161101. [CrossRef]
52. Sun, J.; Remsing, R.C.; Zhang, Y.; Sun, Z.; Ruzsinszky, A.; Peng, H.; Yang, Z.; Paul, A.; Waghmare, U.; Wu, X.; et al. Accurate first-principles structures and energies of diversely bonded systems from an efficient density functional. *Nat. Chem.* **2016**, *8*, 831–836. [CrossRef]
53. Lee, M.H. Improved Optimised Pseudopotentials and Application to Disorder in γ-Al_2O_3. Ph.D. Thesis, Cambridge University, Cambridge, UK, 1996.
54. Monkhorst, H.J.; Pack, J.D. Special points for Brillouin-zone integrations. *Phys. Rev. B* **1976**, *13*, 5188–5192. [CrossRef]
55. Bellaiche, L.; Vanderbilt, D. Virtual crystal approximation revisited: Application to dielectric and piezoelectric properties of perovskites. *Phys. Rev. B* **2000**, *61*, 7877. [CrossRef]
56. Atuchin, V.V.; Gavrilova, T.A.; Grivel, J.-C.; Kesler, V.G. Electronic structure of layered titanate $Nd_2Ti_2O_7$. *Surf. Sci.* **2008**, *602*, 3095–3099. [CrossRef]
57. Atuchin, V.V.; Bazarov, B.G.; Gavrilova, T.A.; Grossman, V.G.; Molokeev, M.S.; Bazarova, Z.G. Preparation and structural properties of nonlinear optical borates $K_{2(1-x)}Rb_{2x}Al_2B_2O_7$, $0 < x < 0.75$. *J. Alloys Compd.* **2012**, *515*, 119–122.
58. Hazen, R.M.; Finger, L.W.; Mariathasan, J.W.E. High pressure crystal chemistry of scheelite-type tungstates and molybdates. *J. Phys. Chem. Solids* **1985**, *46*, 253–263. [CrossRef]
59. Stevens, S.B.; Morrison, C.A.; Allik, T.H.; Rheingold, A.L.; Haggerty, B.S. $NaLa(MoO_4)_2$ as a laser host material. *Phys. Rev. B Condens. Matter.* **1991**, *43*, 7386–7394. [CrossRef] [PubMed]
60. Bouzidi, C.; Horchani-Naifer, K.; Khadraoui, Z.; Elhouichet, H.; Ferid, M. Synthesis, characterization and DFT calculations of electronic and optical properties of $CaMoO_4$. *Phys. B Condens. Matter* **2016**, *497*, 34–38. [CrossRef]
61. Marques, V.S.; Cavalcante, L.S.; Sczancoski, J.C.; Alcantara, A.F.P.; Orlandi, M.O.; Moraes, E.; Longo, E.; Varela, J.A.; Li, M.S.; Santos, M.R.M.C. Effect of Different Solvent Ratios(Water/Ethylene Glycol) on the Growth Process of $CaMoO_4$ Crystals and Their Optical Properties. *Cryst. Growth Des.* **2010**, *10*, 4752–4768. [CrossRef]
62. Gupta, S.K.; Sahu, M.; Ghosh, P.S.; Tyagi, D.; Saxena, M.K.; Kadam, R.M. Energy transfer dynamics and luminescence properties of Eu^{3+} in $CaMoO_4$ and $SrMoO_4$. *Dalton Trans.* **2015**, *44*, 18957–18969. [CrossRef]
63. Tranquilin, R.L.; Oliveira, M.C.; Santiago, A.A.G.; Lovisa, L.X.; Ribeiro, R.A.P.; Longo, E.; de Lazaro, S.R.; Almeida, C.R.R.; Paskocimas, C.A.; Motta, F.V.; et al. Presence of excited electronic states on terbium incorporation in $CaMoO_4$: Insights from experimental synthesis and first-principles calculations. *J. Phys. Chem. Solids* **2021**, *149*, 109790. [CrossRef]